

SHAPE FROM FOCUS

k.kanthamma*, Dr S.A.K.Jilani**

*(Department of electronics and communication engineering, srinivasa ramanujan institute of technology,
Anantapur,Andrapradesh,INDIA

** (Department of electronics and communication engineering, madanapalle institute of technology and science,
Madanapalle,Andrapradesh,INDIA

Abstract—

this paper presents the shape from focus here uses different focus levels to obtain a sequence of object images. The sum-modified-Laplacian(SML) operator is developed to provide local measures of the quality of image focus. The operator is applied to the image sequence to determine a set of Focus measures at each image. Point a depth estimation algorithm interpolates a small number of focus measure values to obtain accurate depth estimates. Results are presented that the accuracy and robustness of the proposed method. These results suggest shape from focus to be an effective approach for variety of challenging visual inspection problems.

Keywords—defocus, focus operator, focus measure function, depth estimation, roughness and texture, automatic shapefromfocus.

I. INTRODUCTION

All surfaces encountered in practice are rough at some level of detail. At that level, they exhibit high frequency spatial surface variations which are random in nature. The recovery problem often associated with rough surfaces. In many vision applications, the spatial surface variations are comparable in dimensions to the resolution of the imaging system. This is the most often the case with microscopic objects where a few microns of surface area can occupy an entire digital image. Image intensities produced by such surfaces vary in an unpredictable manner from pixel to pixel. Hence, It is difficult to obtain dense accurate surface shape information by using existing passive & active sensing techniques, such as binocular stereo, shape from shading, photometric stereo and structured light. We develop a shape recovery technique that uses focus analysis to compute the dense depth maps of rough textured surfaces. Focusing mechanism play a vital role in the human vision system. Focus analysis has been used to automatically focus imaging systems or to obtain sparse depth information from the observed scene. We show that focus analysis can be put to great use by restricting ourselves to a particular class of surfaces. These are the surfaces that produce textured images either due to their roughness or due to reflectance variations. The sum modified laplacian(SML) operator is developed to measure the relative degree of focus between images. the operator is applied to the image sequence to obtain a set of focus measures at each image point. Focus measure variations due to

defocusing can be approximated using Gaussian model.

II. FOCUSED AND DEFOCUSED IMAGES

Fundamental to the concept of recovering shape by focus analysis is the relationship between focused and defocused images of a scene. In this section, we briefly review the image formation process and describe defocused images as processed versions of focused ones. Figure 1 shows the basic image formation geometry.

All light rays that are radiated by the object point P and intercepted by the lens are refracted by the lens to converge at the point Q on the image plane. For a thin lens, the relationship between the object distance o , focal distance of the lens f , and the image distance i , is given by the Gaussian lens law:

$$\frac{1}{o} + \frac{1}{i} = \frac{1}{f} \quad (1)$$

Each point on the object plane is projected onto a single point on the image plane, thus causing a clear or focused image $I_f(x,y)$ to be formed on the image plane. If, however, the sensor plane does not coincide with the image plane and is displaced from it by a distance δ , the energy received from the object by the lens is distributed over a circular patch on the sensor plane. Fig. 1 may be used to

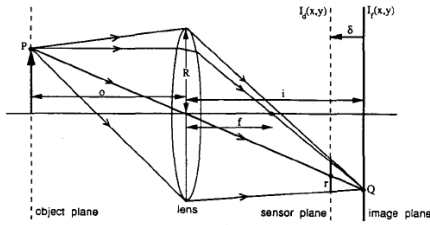


Fig. 1. Formation of focused and defocused images.

establish the following relationship between the radius r of the circular patch and the sensor displacement δ :

$$r = \frac{\delta R}{i} \quad (2)$$

where R is the radius of the lens.

The distribution of light energy over the patch, or the **blurring function**, can be accurately modeled using physical optics. Very often, a two-dimensional Gaussian function is used to approximate the physical model. Then, the blurred or **defocused** image $I_d(x, y)$ formed on the sensor plane can be described as the result of convolving the focused image $I_f(x, y)$ with the blurring function $h(x, y)$:

$$I_d(x, y) = h(x, y) * I_f(x, y) \quad (3)$$

Where

$$h(x, y) = \frac{1}{2\pi(\sigma_h)^2} e^{-\frac{x^2+y^2}{2\sigma_h^2}} \quad (4)$$

The spread parameter, σ_h , is assumed to be proportional to the radius r . The constant of proportionality is dependent on the imaging optics and the image sensor. We will see shortly that the value of this constant is not important in our approach. Note that defocusing is observed for both positive and negative sensor displacements. Now consider the defocusing process in frequency domain (u, v). If $I_f(u, v)$, $H(u, v)$, and $I_d(u, v)$ are the Fourier transforms of $I_f(x, y)$, $h(x, y)$, and $I_d(x, y)$, respectively, we can express (3) as

$$I_D(u, v) = H(u, v) \cdot I_F(u, v) \quad (5)$$

Where

$$H(u, v) = e^{-\frac{u^2+v^2}{2}(\sigma_h)^2} \quad (6)$$

We see that $H(u, v)$ allows low frequencies to pass while it attenuates the high frequencies in the focused image. Furthermore, as the sensor displacement δ increases, the defocusing radius r

increases, and the spread parameter σ_h increases. Hence defocusing is a low-pass filtering process

where the bandwidth decreases with increase in defocusing. From Fig. 1, it is seen that a defocused image of the object can be obtained in three ways: by displacing the sensor with respect to the image plane, by moving the lens, or by moving the object with respect to the object plane. Moving the lens or sensor with respect to one another causes the following problems.

- The magnification of the system varies, causing the image coordinates of focused points on the object to change.
- The area on the sensor over which light energy is distributed varies, causing a variation in image brightness.

In order to overcome these problems, we propose varying the degree of focus by moving the object with respect to a fixed configuration of the optical system and sensor.

III.SHAPE FROM FOCUS

Figure.2 shows a surface of unknown shape placed on a translational stage. The reference plane shown corresponds to the initial position of the stage. The configuration of the optics and sensor defines a single plane, the "focused plane" that is perfectly focused onto the sensor plane. The distance d_f between the focused and reference planes, and the displacement d of the stage with respect to the reference plane, are always known by measurement. Consider the surface element s , that lies on the unknown surface S . If the stage is moved towards the focused plane, the image of s will gradually increase in its degree of focus (high-frequency content) and will be perfectly focused when s lies on the focused plane. Further movement of the element s will again increase the defocusing of its image. If we observe the image area corresponding to s and record the stage displacement $d = d^1$ at the instant of maximum focus, the height d_s of s with respect to the stage can be computed as $d_s = d_f - d^1$. This procedure may be applied independently to all surface elements to obtain the shape of the entire surface S . To automatically detect the instant of "best" focus, an image focus measure will be developed.

In the above discussion, the stage motion and image acquisition were assumed to be continuous processes. In practice, however, it is not feasible to acquire and process such a large number of images in a reasonable amount of time.

Therefore, only a small number of images are used; the stage is moved in increments of Δd , and an image is obtained at each stage position ($d = n \cdot \Delta d$).

By studying the behavior of the focus measure, an interpolation method is developed that uses only a small number of focus measures to obtain accurate depth estimates. An important feature of the proposed method is its local nature; the depth estimate at an image point is computed only from focus measures recorded at that point. Consequently, it can adapt well to texture variations over the object surface.

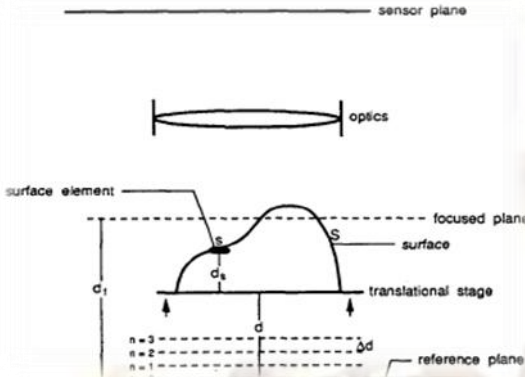


Fig: 2. Shape from focus

IV. A FOCUS MEASURE OPERATOR

To measure the quality of focus in a small image area, we develop a focus measure operator. The operator must respond to high-frequency variations in image intensity, and ideally, must produce maximum response when the image area is perfectly focused.

Generally, the objective has been to find an operator that behaves in a stable and robust manner over a variety of images, including those of indoor and outdoor scenes. Such an approach is essential while developing automatically focusing systems that have to deal with general scenes.

Equation (3) relates a defocused image to a focused image using the blurring function. Assume that a focus measure operator $o(x, y)$ is applied (by convolution) to the defocused image $I_d(x, y)$. The result is a new image $r(x, y)$ that may be expressed as

$$r(x, y) = o(x, y) * (h(x, y) * I_f(x, y)) \tag{7}$$

Since convolution is linear and shift-invariant, we can rewrite the above expression as

$$r(x, y) = h(x, y) * (o(x, y) * I_f(x, y)) \tag{8}$$

Therefore, applying a focus measure operator to a defocused image is equivalent to defocusing a new image obtained by convolving the focused image with the operator. The operator only selects the frequencies in the focused image that will be attenuated due to defocusing. Since defocusing is a low-pass filtering process, its effects on the image are more pronounced and detectable if the image has

strong high-frequency content. An effective focus measure operator, therefore, must high-pass filter the image.

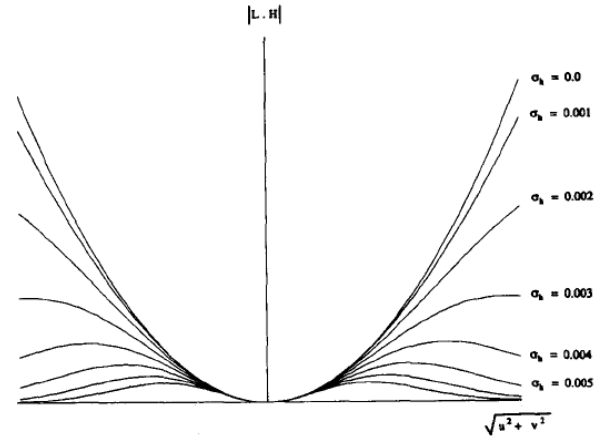


Fig:3. The effect of defocusing and second-order differentiation in frequency domain.

One way to high-pass filter an image is to determine its second derivative. For two-dimensional images, the Laplacian may be used:

$$\nabla^2 I = \frac{\partial^2 I}{\partial x^2} + \frac{\partial^2 I}{\partial y^2} \tag{9}$$

In frequency domain, applying the Laplacian $L(u, v)$ to the defocused image $I_D(u, v)$ (5) gives

$$L(u, v) \cdot H(u, v) \cdot I_f(u, v) \tag{10}$$

where

$$L(u, v) \cdot H(u, v) = -(u^2 + v^2) \cdot e^{-\frac{u^2 + v^2}{2} \sigma_h^2} \tag{11}$$

Fig. 3 shows the frequency distribution of $L.H/$ for different values of the defocusing parameter σ_h . For any given frequency (u, v) , $L.H/$ varies as a Gaussian function of σ_h . In general, however, the result would depend on the frequency distribution of the imaged scene. Though our texture is random, it may be assumed to have a set of dominant frequencies. Then, loosely speaking, each frequency is attenuated by a Gaussian function in σ_h and its width is determined by the frequency. Therefore, the result of applying the Laplacian operator may be expressed as a sum of Gaussian functions in σ_h . The result is expected to be maximum when $\sigma_h = 0$, i.e., when the image is perfectly focused. Since the frequency distribution of the texture is random, the widths of the Gaussian functions are also random. Using central limit theorem, the result of applying the Laplacian operator to an image point may be assumed to be a Gaussian function of the defocus parameter σ_h .

We note that in the case of the Laplacian the second derivatives in the x and y directions can have opposite signs and tend to cancel each other. In the case of textured images, this phenomenon may occur frequently and the Laplacian may at times behave in an unstable manner. We overcome this problem by defining the modified Laplacian as

$$\nabla^2_M I = \left| \frac{\partial^2 I}{\partial x^2} \right| + \left| \frac{\partial^2 I}{\partial y^2} \right|. \quad (12)$$

Hence, a discrete approximation to the modified Laplacian is obtained as

$$ML(x, y) = | 2I(x, y) - I(x - \text{step}, y) - I(x + \text{step}, y) | + | 2I(x, y) - I(x, y - \text{step}) - I(x, y + \text{step}) |. \quad (13)$$

Finally, the focus measure at a point (i, j) is computed as the sum of modified Laplacian values, in a small window around (i, j) , that are greater than a threshold value:

$$F(i, j) = \sum_{x=i-N}^{i+N} \sum_{y=j-N}^{j+N} ML(x, y) \text{ for } ML(x, y) \geq T_1. \quad (14)$$

The parameter N determines the window size used to compute the focus measure. In contrast to auto-focusing methods, we typically use a small window of size 3×3 or 5×5 , i.e., $N = 1$ or $N = 2$. We shall refer to the above focus measure as the *sum-modified-laplacian* (SML).

V.EVALUATING THE FOCUS MEASURE

We evaluate the SML focus measure by analyzing its behavior as a function of the distance between the observed surface and the focused plane. In Fig. 4, the focus measure functions of two samples are shown. Sample X has high texture content while sample Y has relatively weaker texture. Both samples are made of a paste containing resin and tungsten particles. The variable size of the tungsten particles gives the surfaces a randomly textured appearance. For each sample, the stage is moved in increments (Δd) of 1 micro meter, an image of the sample is obtained, and the SML measure is computed using an evaluation window of 10×10 pixels. The vertical lines in Fig. 4 indicate the known initial distances ($d_f - d_s$) of the samples from the focused plane. The focus measures were computed using parameter values of $\text{step} = 1$ and $TI = 7$. No form of temporal filtering was used to reduce the effects of image noise. Though the measure values are slightly noisy, they peak very close to the expected peak positions (vertical lines). We see that the focus measure function peaks sharply for the stronger texture but relatively slowly and with a lower peak value for the weaker texture. The sharpness of the focus measure function depends not only on the

texture strength but also the depth of field of the imaging system. The depth of field, in turn, depends on the magnification and aperture size of the imaging optics as well as the physical resolution of the sensor. A smaller depth of field causes the focus quality of the image to vary more rapidly with object motion, causing a sharper peak.

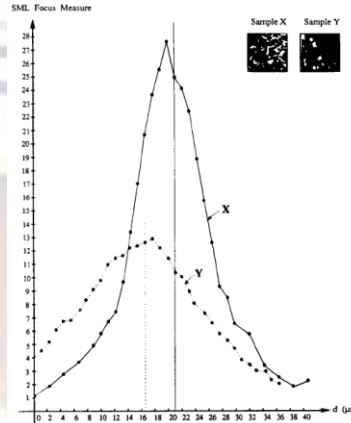


Fig.4. SML focus measure function computed for two texture samples.

VI.DEPTH ESTIMATION

we now describe the estimation of depth \bar{d} of a surface point (x, y) from the focus measure set $\{f(d_i) \text{ where } i=1, 2, \dots, M\}$. For convenience the notation F_i is used in place of $f(d_i)$. A coarse depth may be obtained by using an algorithm that simply looks for the displacement value d , that maximizes the focus measure and assigns that value to \bar{d} . A more accurate depth map is obtained by using the Gaussian distribution to interpolate the focus measures. The interpolation is done using only three focus measures, namely, F_{m-1}, F_m, F_{m+1} , that lie on the largest mode of $F(d)$, such that, $F_m \geq F_{m-1}$ and $F_m \geq F_{m+1}$.

Using the Gaussian model, focus measure function may be expressed as:

$$F = F_p \exp \left\{ -\frac{1}{2} \left(\frac{d - \bar{d}}{\sigma_F} \right)^2 \right\} \quad (15)$$

where \bar{d} and σ_F are the mean and standard deviation of the Gaussian distribution

Using natural logarithm, we have:

$$\ln F = \ln F_p - \frac{1}{2} \left(\frac{d - \bar{d}}{\sigma_F} \right)^2. \quad (16)$$

By substituting each of three measures F_{m-1}, F_m, F_{m+1} , and its corresponding displacement value in (16), we obtain a set of equations that can be solved for \bar{d} and σ_F :

$$\bar{d} = \frac{(\ln F_m - \ln F_{m+1})(d_m^2 - d_{m-1}^2)}{2 \Delta d \{(\ln F_m - \ln F_{m-1}) + (\ln F_m - \ln F_{m+1})\}} \quad (17)$$

$$\sigma_F^2 = -\frac{(d_m^2 - d_{m-1}^2) + (d_m^2 - d_{m+1}^2)}{2 \{(\ln F_m - \ln F_{m-1}) + (\ln F_m - \ln F_{m+1})\}} \quad (18)$$

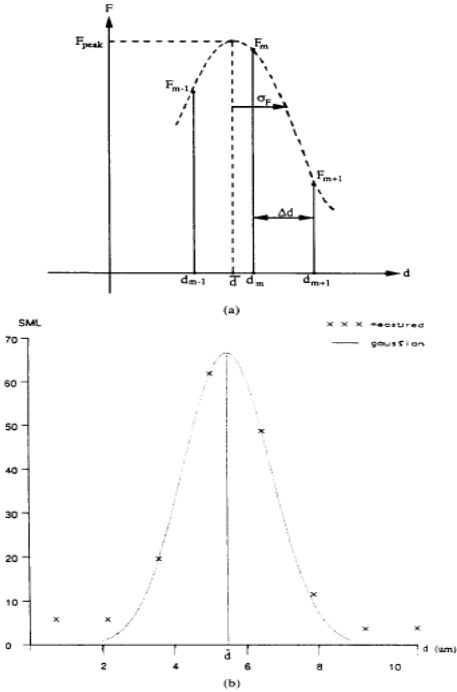


Fig:5. Depth estimation : (a) Gaussian interpolation of focus measures ; (b) experimental result

If F_p is large and σ_F is small, the focus measure function has a strong peak, indicating high surface texture content in the vicinity of the image point (x, y) . Thus, F_p and σ_F may be used to segment the observed scene into regions of different textures. Fig. 5(b) shows the experimental result of Gaussian interpolation applied to a real sample. Hence, the parameter values corresponding to all possible sets of the three focus measures can be computed a-priori and stored in a table. Given any set of focus measures, the corresponding parameter values are simply read from the table. However, the displacement parameter Δd is not fixed and may vary from one application to another. In order to generate look-up tables that are independent of Δd and the depth \bar{d} , we define the normalized focus measures:

$$\hat{F}_{m-1} = \frac{F_{m-1}}{F_m}, \quad \hat{F}_m = 1, \quad \hat{F}_{m+1} = \frac{F_{m+1}}{F_m} \quad (20)$$

And the corresponding displacement values:

$$\hat{d}_{m-1} = -1, \quad \hat{d}_m = 0, \quad \hat{d}_{m+1} = 1. \quad (21)$$

The parameters of this Gaussian are the mean value \bar{d} , standard deviation σ_F , and peak value F_p . The correspondence between the normalized measures F_{m-1} and F_{m+1} and the parameters \bar{d} , σ_F , and F_p are precomputed using (17)-(19), respectively, and stored as three two dimensional look-up tables. During depth estimation, the computed focus measures F_{m-1} and F_{m+1} are normalized to determine \hat{F}_{m-1} and \hat{F}_{m+1} . These normalized measures are used to index the look-up tables and determine the parameters \bar{d} , σ_F , and F_p . The parameters of the original Gaussian function are then determined as:

$$\bar{d} = d_m + \Delta d \hat{d}, \quad \sigma_F = \Delta d \hat{\sigma}_F, \quad F_p = F_m \hat{F}_p. \quad (22)$$

During run time, the use of look-up tables saves the computations involved in the evaluation of \bar{d} , F_p , and σ_F using (17)-(19).

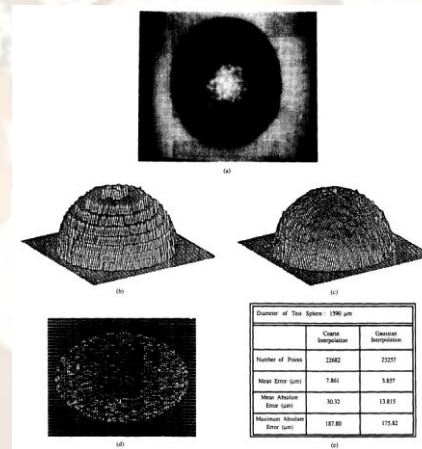


Fig:6 . Experimental result; steel ball. The known shape of the ball is used to analyze errors in the depth maps computed using the coarse resolution and Gaussian interpolation algorithm. (a) camera image; (b)Depth map: coarse resolution; (c) Depth Map : Gaussian interpolation ; (d) Error map: Gaussian interpolation ; (e) Error statistics.

VII.AUTOMATED SHAPE FROM FOCUS SYSTEM

A photograph of the system is shown in Fig. 7. Objects are imaged using a Nikon Alphaphot-2 model microscope and a CCD camera with 512x480 pixels. Magnification of the complete imaging system can be varied using objective lenses of different powers (x 10, x40, or x 100). Bright field illumination is used to illuminate the object: light energy is focused on the object via the same lenses that are used to image it.

The z-axis of the microscope stage is driven by a stepper motor and the position of the stage can be computer controlled with a resolution and accuracy of 0.02 μm . The shape from focus algorithm is programmed and executed on a Sun SPARC 2 workstation. The complete recovery process including image acquisition, focus measure computation, and depth estimation takes a total of about 40 seconds for a sequence of 10 input image.

We estimate that by using fairly simple customized hardware this recovery process can be accomplished in less than 1 second.



Fig. 7. Automated shape from focus system.

Prior to automating the shape from focus system, experiments were conducted to determine the accuracy and feasibility of the method. In these experiments, the microscope stage was moved manually and a sequence of images obtained and processed using both the coares resolution and Gaussian interpolation depth recovery algorithms.

The first experiment was conducted on a steel ball sample that is 1590 μm in diameter. The ball has a rough surface that gives it a textured appearance. A camera image of the ball, under bright held illumination, is shown in Fig. 6(a). Due to the small depth of field of the microscope, some areas of the ball are defocused. An incremental displacement of $\Delta d = 100 \mu\text{m}$ was used to take 1.3 images of the ball. A 5 x 5 SML operator (with $\text{TI} = 7$ and $\text{step} = 1$) was applied to the image sequence to obtain focus measures. The coarse resolution depth map in Fig. 6(b) is computed by simply assigning to each surface point the depth value corresponding to the stage position that produced the maximum focus measure. Fig. 6(c) show the depth map obtained using Gaussian interpolation.

The known size and location of the ball were used to compute error maps from the two depth maps. The error map for the Gaussian interpolation algorithm is shown in Fig. 6(d). The accuracy of the method depends on several factors: surface texture, depth of field of the imaging system, and the incremental displacement Δd . The automated system has been used to recover the shapes of a variety of industrial as well

as biological samples. Fig. 8 shows a tungsten paste filling in a via-hole on a ceramic substrate. These fillings are used to establish electrical connections between components on multilayered circuit boards. Fig. 8 has a cavity, indicating lack of filling. The specular reflectance and variable size of the tungsten particles gives the surface a random texture. In this case, a total of 18 images were taken using stage position increments of 8 μm . Some of these images are shown in Fig. 8(a)-(f). Fig. 8(g) and Fig. 8(h) show a reconstructed image and two views of the depth map, respectively. The image reconstruction algorithm simply uses the estimated depth to locate and patch together the best focused image areas in image sequence.

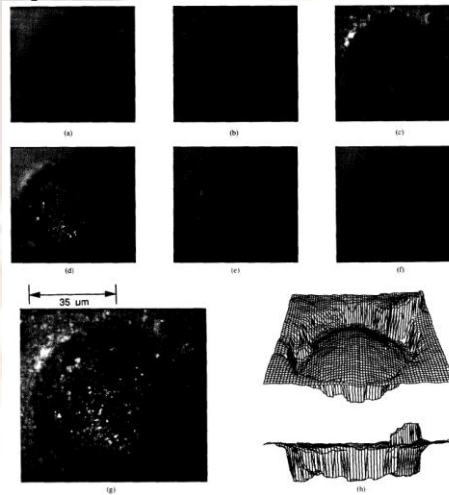


Fig:8. Result obtained using the automated system: via-hole filling on a ceramic substrate. The via-hole is approximately 70 micro meter and has insufficient filling. (a) $i=2$; (b) $i=5$; (c) $i=8$; (d) $i=11$; (e) $i=14$; (f) $i=18$; (g) Reconstructed image; (h) Depth maps.

VIII.CONCLUSION

The above experiments demonstrate the effectiveness of the shape from focus method. Small errors in computed depth estimates result from factors such as, image noise, Gaussian approximation of the SML focus measure function, and weak textures in some image areas. Some detail of the surface roughness is lost due to the use of a finite size window to compute focus measures. The above experiments were conducted on microscopic surfaces that produce complex textured images. Such images are difficult, if not impossible, to analyze using recovery techniques such as shape from shading, photometric stereo, and structured light. These techniques work on surfaces with simple reflectance properties. Since the samples are microscopic in size, it is also difficult to use binocular stereo. Methods for recovering shape by texture

analysis have been researched in the past. Typically, these methods recover shape information by analyzing the distortions in image texture due to surface orientation. The underlying assumption is that the surface texture has some regularity to it. Clearly, these approaches are not textures. For these reasons, shape from focus may be viewed as an effective method for objects with complex surface characteristics.

REFERENCES

- [1] S.K. Nayar and y. nakagawa, "*shape from focus*" *tech.rep ,dept,ofcompt.sci.*, Columbia univ.,CUCS 058-92,nov,1992.
- [2] M.subbarao and g.surya, "*depth from defocus:a spatial domain approach*," Tech. Rep 92.12.03, SUNY, stony brook, Dec, 1992
- [3] E. Krotkov, *Active Computer Vision by cooperative Focus and Stereo*, Springer-Verlag, New York, 1989
- [4] B.K.P.Horn, *Robot Vision*, MIT Press, 1986
- [5] M. Subbs Rao "*Efficient depth recovery through inverse optics*" Mission Vision for Inspection and Magerment. H.freeman, Ed, New YorkAcademic press,1989.
- [6] J.M.Tenenbaum, "*Accommodation in computer vision*", Ph.D, thesis, Stanford Univ, 1970
- [7] N. Ahuja and L.Abbott, "*Active Stereo: Integrating Disparity, Vergence, Focus, Aperture, and Calibration for Surface Estimation*," , PAMI, vol. 15, no. 10, Oct. 1993, pp.1007-1029.
- [8] J.Ens and p.lawrence, "*An investigation of Methods for Determining depth from focus*," *PAMI*,vol. 15, no. 2,pp, 97-107,1993.